

## Lipschitz and Total-Variational Regularization for Blind Deconvolution

Yu-Mei Huang<sup>1,2</sup> and Michael K. Ng<sup>1,\*</sup>

<sup>1</sup> Centre for Mathematical Imaging and Vision and Department of Mathematics, Hong Kong Baptist University, Kowloon Tong, Hong Kong.

<sup>2</sup> Department of Mathematics, Lanzhou University, Gansu, China.

Received 3 June 2007; Accepted (in revised version) 9 November 2007

Communicated by Pingwen Zhang

Available online 27 February 2008

---

**Abstract.** In [3], Chan and Wong proposed to use total variational regularization for both images and point spread functions in blind deconvolution. Their experimental results show that the detail of the restored images cannot be recovered. In this paper, we consider images in Lipschitz spaces, and propose to use Lipschitz regularization for images and total variational regularization for point spread functions in blind deconvolution. Our experimental results show that such combination of Lipschitz and total variational regularization methods can recover both images and point spread functions quite well.

**AMS subject classifications:** 52B10, 65D18, 68U05, 68U07

**Key words:** Lipschitz regularization, total variational regularization, blind deconvolution, texture, Poisson singular integral, alternating iterative algorithm.

---

## 1 Introduction

It is well-known that recovering both an image  $u$  and a point spread function (PSF)  $k$  is a mathematically ill-posed problem. This is called a blind deconvolution problem. In the literature, there are many methods for simultaneously recovering both  $u$  and  $k$ , see for instance [3, 6, 8, 9, 12, 13]. In [3], Chan and Wong proposed to use total variational (TV) regularization for both images and PSFs in blind deconvolution. The motivation for using TV regularization for the PSF is due to the fact that some PSFs can have edges, see [3]. They find  $u$  and  $k$  by minimizing the cost function defined as follows:

$$\min_{(u,k)} E(u,k) = \min_{(u,k)} \{ \|k * u - f\|_2^2 + \alpha_1 \int |\nabla u| + \alpha_2 \int |\nabla k| \}. \quad (1.1)$$

---

\*Corresponding author. Email addresses: ymhuang@math.hkbu.edu.hk (Y. M. Huang), mng@math.hkbu.edu.hk (M. K. Ng)

Here  $*$  denotes convolution operator,  $u$  and  $k$  are the original image and the exact blur respectively,  $f$  is the observed image,  $\alpha_1$  and  $\alpha_2$  are positive parameters which measure the trade off between a good fit and the regularity of the solutions  $u$  and  $k$ . Chan and Wong devised fast numerical algorithms for solving the minimization problem (1.1). Their algorithm can recover both the image and PSF without any a priori information on the PSF. However, their experimental results show that the detail of the restored images cannot be recovered. The main reason is the TV regularization is used for the image.

In this paper, we consider images in Lipschitz spaces where a wide class of nonsmooth images can be modeled, see for instance [1,4,5], and propose to use Lipschitz regularization for  $u$  and total variational regularization for  $k$  in blind deconvolution. Similar to (1.1), we formulate the blind deconvolution problem as follows:

$$\min_{(u,k)} E(u,k) = \min_{(u,k)} \{ \|k*u - f\|_2^2 + \alpha_1 (\|u\|_2^2 + \gamma \|z_t*u\|_2^2) + \alpha_2 \int |\nabla k| \}, \quad (1.2)$$

where  $\alpha_1$  and  $\alpha_2$  are the regularization parameters, and the image regularization term based on the Wiener filtering is given by  $(\|u\|_2^2 + \gamma \|z_t*u\|_2^2)$ , see [1] for detail. Here  $z_t$  ( $t > 0$ ) is a function related to the Poisson kernel used to calibrate the lack of smoothness of  $u$  at the scale  $t$  with the weighting  $\gamma > 0$ . The construction of image regularization term is based on the assumption that the images belong to proper Lipschitz spaces.

The outline of this paper is as follows. In Section 2, we will introduce Lipschitz regularization method and consider alternating minimization algorithm for solving (1.2). In Section 3, numerical results will be presented. Our experimental results show that such combination of Lipschitz and total variational regularization methods can recover both images and point spread functions quite well. The detail of the restored images can be recovered. Finally, the concluding remarks are given in Section 4.

## 2 Blind deconvolution by Lipschitz regularization

Total variational regularization method can efficiently recover edges of images, it loses much fine scales of the images due to the assumption that images are represented by bounded variation functions [7]. In this paper, we consider images in Lipschitz spaces. In order to represent images in Lipschitz spaces, the Poisson singular integral is used to measure the smoothness of an image. The details can be found in [1].

The Poisson singular integral operator is defined as a linear operator on  $L^2(\mathbf{R}^2)$  as follows:

$$\Psi_t u(x,y) = \int_{\mathbf{R}^2} \psi_t(w,v) u(x-w,y-v) dw dv. \quad (2.1)$$

For fixed  $t > 0$ , the Poisson kernel  $\psi_t(x,y)$  is given by

$$\psi_t(x,y) = \frac{t}{2\pi(x^2+y^2+t^2)^{3/2}}, \quad \forall (x,y) \in \mathbf{R}^2. \quad (2.2)$$

We note that a function  $u$  is in Lipschitz space if and only if

$$\sup_{t>0} t^{-\beta} \|\Psi_t u - u\|_2 < \infty, \tag{2.3}$$

where  $\|\cdot\|_2$  is the  $L^2$ -norm and  $\beta$  is the parameter of Lipschitz space which image  $u$  belongs to. The value of  $\beta$  reflects the degree of smoothness of image  $u$ , smoother the image  $u$  is, larger the parameter  $\beta$  will be. In practice, we can compute the following integral

$$\int_0^t \|\Psi_s u - u\|_2^2 ds$$

to calibrate the lack of smoothness of  $u$ . Because the Fourier transform of  $\psi_t(x, y, t)$  is  $e^{-t\rho}$  ( $\rho = \sqrt{\xi^2 + \eta^2}$ ), by using the Parseval theorem, we obtain

$$\int_0^t \|\Psi_s u - u\|_2^2 ds = \int_{\mathbf{R}^2} \int_0^t (1 - e^{-s\rho})^2 ds |\hat{u}(\xi, \eta)|^2 d\xi d\eta,$$

where  $\hat{u}$  denotes the Fourier transform of  $u$ . Using convolution theorem and Parseval theorem again, it implies that

$$\begin{aligned} \int_0^t \|\Psi_s u - u\|_2^2 ds &= \int_{\mathbf{R}^2} |\hat{z}_t(\xi, \eta) \hat{u}(\xi, \eta)|^2 d\xi d\eta \\ &= \|\mathcal{F}^{-1}(\hat{z}_t(\xi, \eta) \hat{u}(\xi, \eta))\|_2^2 = \|z_t * u\|_2^2, \end{aligned}$$

where  $\mathcal{F}^{-1}$  is the inverse Fourier transform operator,  $*$  is the convolution operator,  $z_t$  is the inverse Fourier transform of  $\hat{z}_t$ , and

$$\hat{z}_t(\xi, \eta) = \left\{ \int_0^t (1 - e^{-s\rho})^2 ds \right\}^{1/2} = \left\{ t + \frac{4e^{-t\rho} - e^{-2t\rho} - 3}{2\rho} \right\}^{1/2}, \quad \text{with } \rho = \sqrt{\xi^2 + \eta^2},$$

i.e.,  $\int_0^t \|\Psi_s u - u\|_2^2 ds$  is just the measurement of convolution of  $z_t$  and  $u$ . Therefore when  $u$  is in a Lipschitz space with a certain degree of smoothness, it can be controlled by the magnitude of  $(\|u\|_2^2 + \gamma \|z_t * u\|_2^2)$ . In practice, the image can be viewed as originally defined on a region from which it is extended by periodicity to all of  $\mathbf{R}^2$ . The above results remain valid in the periodic case [1]. Therefore Fast Fourier Transforms (FFTs) can be used to evaluate the above calculation in the Fourier domain efficiently. Other boundary conditions can be used to handle corresponding background situations [10]. For instance, when reflective boundary conditions are used, Discrete Cosine Transforms (DCTs) can be applied to calculate the Lipschitz regularization term.

In (1.2), we can minimize the objective function involving the regularization term  $(\|u\|_2^2 + \gamma \|z_t * u\|_2^2)$  because of the image being in a Lipschitz space. In the next section, numerical examples are given to demonstrate that this image regularization term is quite effective in recovery of the detail of an image in blind deconvolution.

To devise numerical algorithm for (1.2), let us write down the first order optimality conditions, that is,

$$\frac{\partial E}{\partial k} = 2u(-x, -y) * (u * k - f) - \alpha_2 \nabla \cdot \frac{\nabla k}{|\nabla k|} = 0, \quad (2.4)$$

and

$$\frac{\partial E}{\partial u} = 2k(-x, -y) * (k * u - f) + 2\alpha_1 (u + \gamma z_t(-x, -y) * (z_t * u)) = 0. \quad (2.5)$$

For (2.4), it can be solved by the lagged diffusivity fixed point iteration, see [11]. We apply preconditioned conjugate gradient method with cosine transform based preconditioners to solve the linear system at each fixed point iteration [2]. For (2.5), it can be solved in Fourier domain by

$$\hat{u}(\xi, \eta) = \frac{\tilde{k}(\xi, \eta) \hat{f}(\xi, \eta)}{|\hat{k}(\xi, \eta)|^2 + \alpha_1 (1 + \gamma |\hat{z}_t|^2)}, \quad (2.6)$$

where  $\hat{u}$ ,  $\hat{k}$ ,  $\hat{f}$  and  $\hat{z}_t$  are the Fourier transforms of  $u$ ,  $k$ ,  $f$  and  $z_t$  respectively. In particular, the  $m$ -by- $m$  image solution  $u$  can be determined in  $\mathcal{O}(m^2 \log m)$  operations by using fast Fourier transforms. Since both PSF and image are unknown, we adopt an alternating iterative algorithm in which the function value  $E(u, k)$  always decreases as the iterations increase. More precisely, the algorithm is stated as follows: With an initial guess  $(u^0, k^0)$ , we first solve  $E(u^0, k^1) \equiv \min_k E(u^0, \cdot)$  from (2.4), then solve  $E(u^1, k^1) \equiv \min_u E(\cdot, k^1)$  using (2.6), and so on, here we let the initial value of  $u^0$  as the observed image. When we set the initial  $k^0$  as delta function, we can calculate  $u$  first instead in the iterative procedure, that is, solve  $E(u^1, k^0) \equiv \min_u E(\cdot, k^0)$  using (2.6) first and then solve  $E(u^1, k^1) \equiv \min_k E(u^1, \cdot)$  from (2.4), and so on. By assuming after getting  $u^n$  and  $k^n$ , we solve for  $k^{n+1}$  from equation

$$2u^n(-x, -y) * (u^n * k^{n+1} - f) - \alpha_2 \nabla \cdot \frac{\nabla k^{n+1}}{|\nabla k^{n+1}|} = 0, \quad (2.7)$$

and solve  $u^{n+1}$  from (2.5) in the Fourier space by:

$$\hat{u}^{n+1}(\xi, \eta) = \frac{\tilde{k}^{n+1}(\xi, \eta) \hat{f}(\xi, \eta)}{|\hat{k}^{n+1}(\xi, \eta)|^2 + \alpha_1 (1 + \gamma |\hat{z}_t|^2)}. \quad (2.8)$$

In addition, as noted in [3], the solution of (1.2) is usually not unique. If  $(u, k)$  is a solution, then  $(-u, -k)$  and  $(u(x \pm c, y \pm d), k(x \mp c, y \mp d))$  are the solutions too, here  $c$  and  $d$  are any real constants. So we add nonnegative constraint to both image  $u$  and PSF  $k$ , and besides we normalize  $k$  and constrain it to be centrosymmetric in each iteration to get a unique solution. That is, solve  $k^{n+1}$  by (2.7), and impose following conditions:

$$\begin{aligned} k^{n+1} &= \begin{cases} k^{n+1}, & \text{if } k^{n+1} > 0, \\ 0, & \text{otherwise,} \end{cases} \\ k^{n+1}(x, y) &= (k^{n+1}(x, y) + k^{n+1}(-x, -y)) / 2, \\ k^{n+1} &= \frac{k^{n+1}}{\int_{\Omega} k^{n+1}(x, y) dx dy}. \end{aligned} \quad (2.9)$$

Solve  $u^{n+1}$  by (2.8), and impose conditions:

$$u^{n+1} = \begin{cases} u^{n+1}, & \text{if } u^{n+1} > 0, \\ 0, & \text{otherwise.} \end{cases} \quad (2.10)$$

### 3 Numerical results

In this section, we illustrate some numerical examples to show the effectiveness of such combination of Lipschitz and total variational regularization methods in blind deconvolution. The results show that the proposed method can recover both images and point spread functions quite well. Improved Signal to Noise ratio (ISNR) and relative error are applied to measure the quality of the restored images. They are defined as follows:

$$\text{ISNR} = 20 * \log_{10} \left( \frac{\|f - u\|_2}{\|\tilde{u} - u\|_2} \right), \quad \text{relative error} = \frac{\|\tilde{u} - u\|_2}{\|u\|_2},$$

where  $u$ ,  $f$  and  $\tilde{u}$  are the original image, the observed image and the recovered image respectively. Relative error of point spread function can be obtained when we set  $u$  and  $\tilde{u}$  as the original and recovered PSF respectively in the expression of relative error.

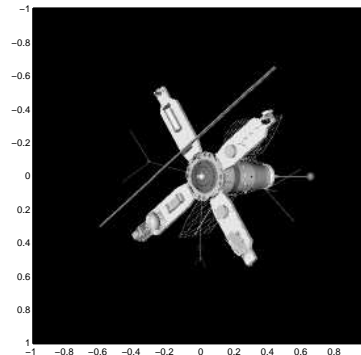


Figure 1: The original satellite image.

The test image is the satellite image shown in Fig. 1 from Philips Laboratory at Kirkland Air Force Base, New Mexico and was provided to us by Professor Robert Plemmons of Wake Forest University. The image consists of 256-by-256 pixels. Currently our codes are written in MATLAB with machine precision roughly equal to  $10^{-16}$ .

In the experiment, we set  $t = 0.1$ , the initial guess for  $u$  is the observed image as it is an only available approximation of  $u$ . We find that the image restoration results can be obtained even other values of  $t$  are used. At each step of alternating iterative algorithm, we iterate the fixed point iteration 50 times. Within each fixed point iteration, we use the preconditioned conjugate gradient method with cosine transform based preconditioners to solve a linear system.

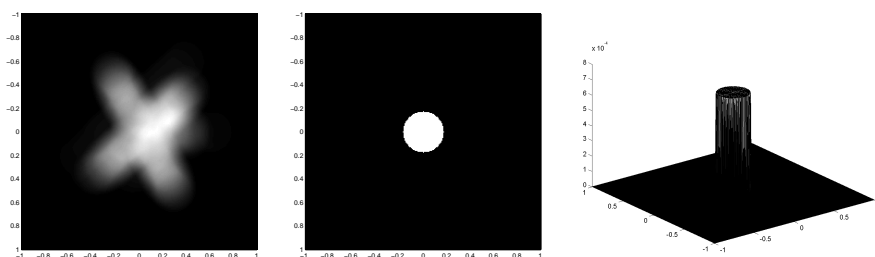


Figure 2: Blurred and noisy image with the relative error = 0.6622 (left), out of focus blur (middle) and the 3D plot of the out of focus blur (right).

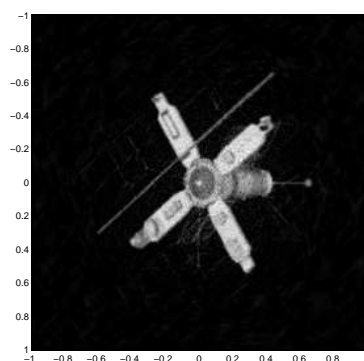


Figure 3: Recovered image with the known PSF, the relative error = 0.2064 and ISNR = 10.1248.

The original image is blurred by a severe defocus blur  $k$  tested in [3] in Fig. 2 (middle), and a blurred image  $f' = k * u$  is generated. In the test, the multiplicative noise given by  $n = 0.005\sigma f'$  (see for instance [1]) are added to the blurred image. Here  $\sigma$  refers to a 256-by-256 uniform random numbers in  $[-1,1]$ . The blurred and noisy image  $f = f' + n$  is shown in Fig. 2 (left). The relative error  $\|u - f\|_2 / \|u\|_2$  of  $f$  is equal to 0.6622. Fig. 3 is the recovered image when the PSF is known. In this test, we set  $\alpha_2 = 0$  (the deconvolution problem) and choose  $\alpha_1 = 1.2 \times 10^{-6}$  by minimizing the relative error  $\|u - u_r\|_2 / \|u\|_2$  of the recovered image  $u_r$ . For the value of  $\gamma$  we used the computed parameters (the value of  $\beta$  and the supremum value of (2.3) in [1]) to set  $\gamma$  being equal to 126.4.

In Fig. 4, we illustrate the ideas on choosing the regularization parameter  $\alpha_2$ . Fig. 4 shows the recovered images and the identified PSFs with their corresponding three-dimensional plots for varies  $\alpha_2$ . The parameters  $\alpha_1$  and  $\gamma$  are fixed at  $1.2 \times 10^{-6}$  and 126.4 as it produces the best recovered image in case the PSF is known. We see that the identified PSF has increasing support as  $\alpha_2$  increases. This result is the same as that in [3]. In Fig. 4, when  $\alpha_2$  is too large, says to  $5 \times 10^{-2}$ , there is nothing recovered, when  $\alpha_2$  is decreasing small to  $10^{-2}$  and  $5 \times 10^{-3}$ , the structure of image can be gotten and the support of the recovered PSF is more bright and the shape of it is close to the exact one. We further decrease  $\alpha_2$  to  $10^{-3}$ , we see the support of recovered PSF is too small and nearly nothing is recovered in the image. We conclude that the optimal  $\alpha_2$  will be in the interval

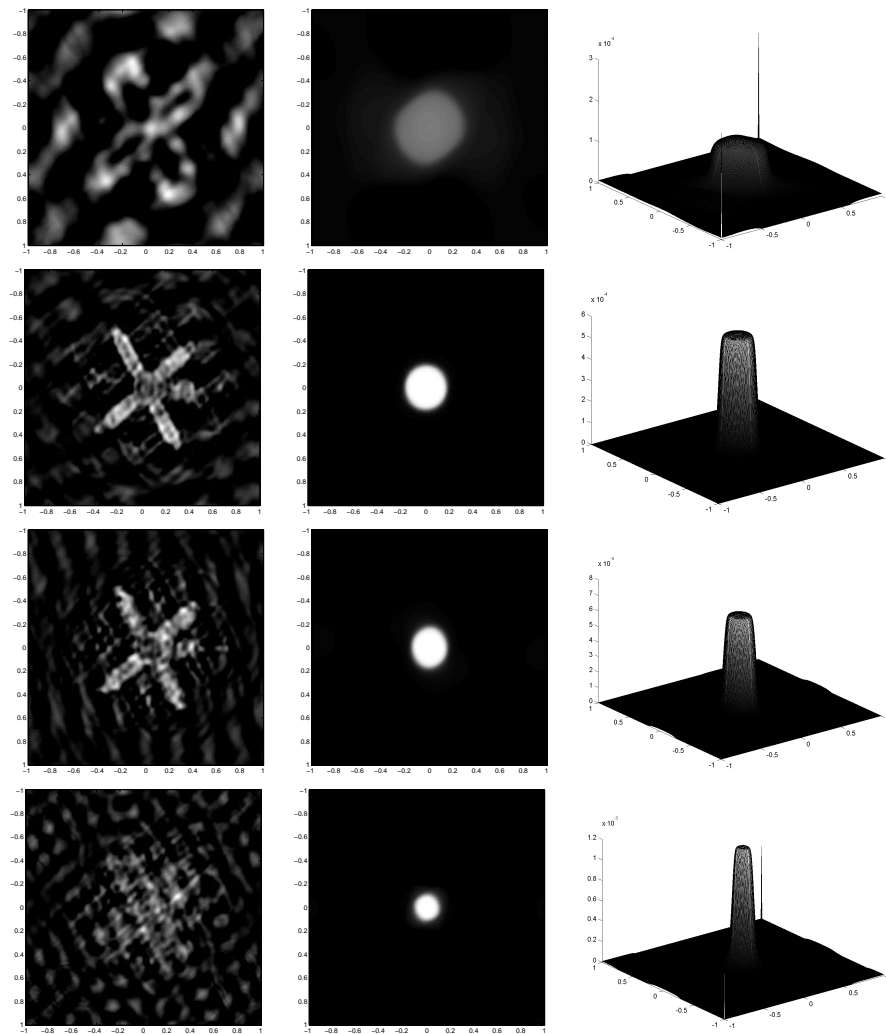


Figure 4: Recovered images (left), recovered PSFs (middle) and their corresponding 3D plots of the recovered PSFs (right) for  $\alpha_2 = 5 \times 10^{-2}, 1 \times 10^{-2}, 5 \times 10^{-3}, 1 \times 10^{-3}$  (from top to bottom).

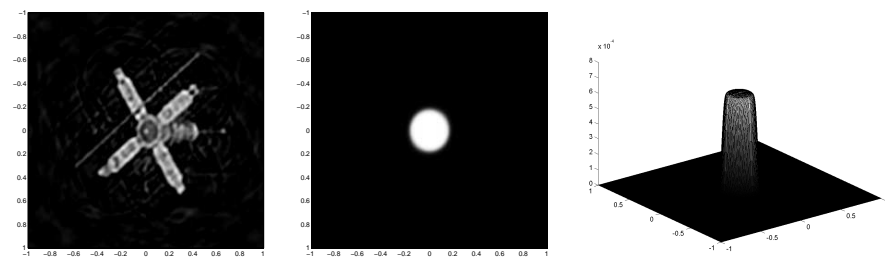


Figure 5: Recovered image (left), recovered PSF (middle) and the corresponding 3D plot of the recovered PSF (right) for  $\alpha_1 = 1.2 \times 10^{-6}$  and  $\alpha_2 = 6.40 \times 10^{-3}$  with the relative error of the recovered image = 0.3545, ISNR=5.4265, and the relative error of the recovered PSF = 0.2055.

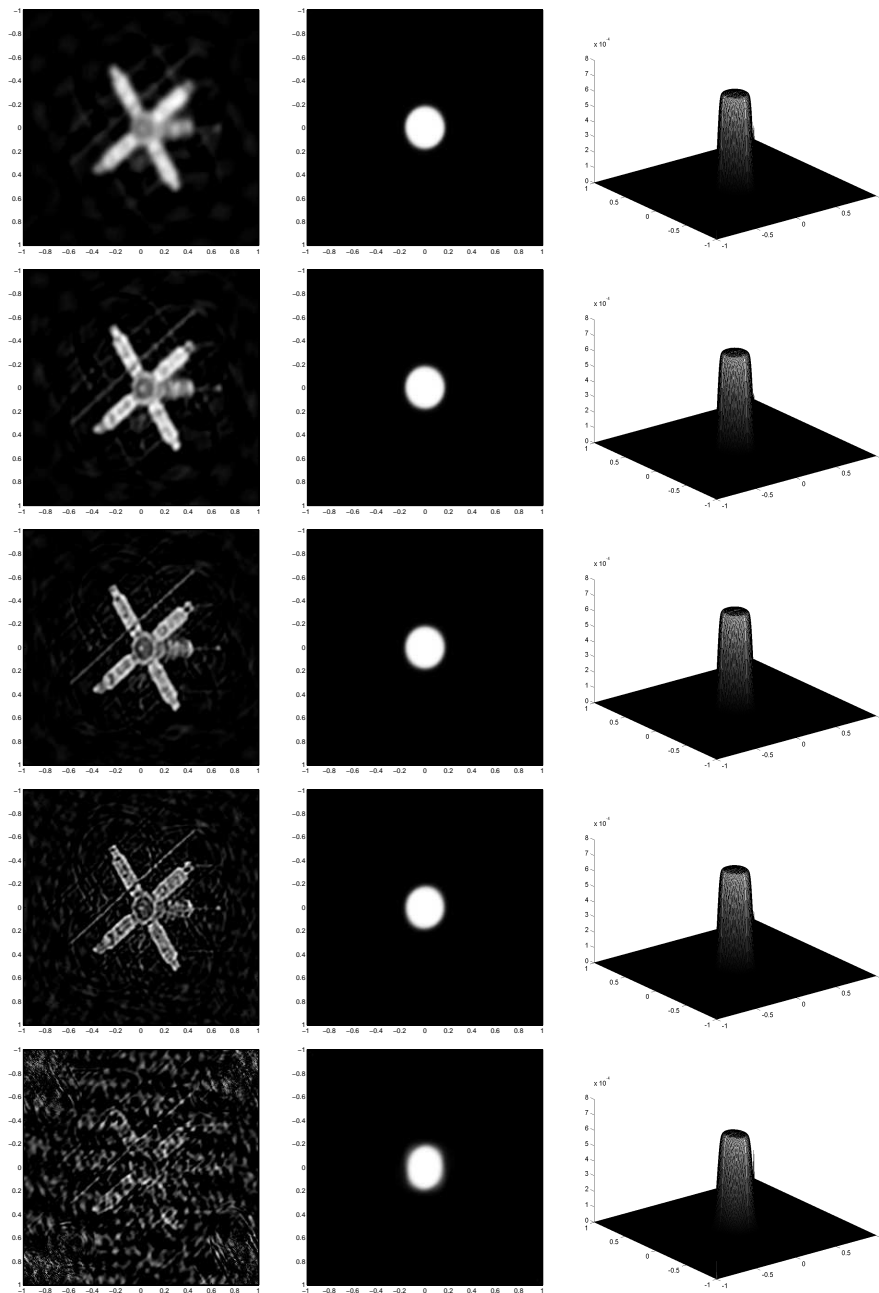


Figure 6: Recovered images (left), recovered PSFs (middle) and their corresponding 3D plots of the recovered PSFs (right) for  $\alpha_1 = 1.2 \times 10^{-4}, 1.2 \times 10^{-5}, 1.2 \times 10^{-6}, 1.2 \times 10^{-7}, 1.2 \times 10^{-8}$  (from top to bottom).

between  $10^{-3}$  and  $10^{-2}$ . By minimizing the relative error of the recovered image, we find that  $\alpha_2 = 6.4 \times 10^{-3}$  gives the best recovered image shown as in Fig. 5. We see that the

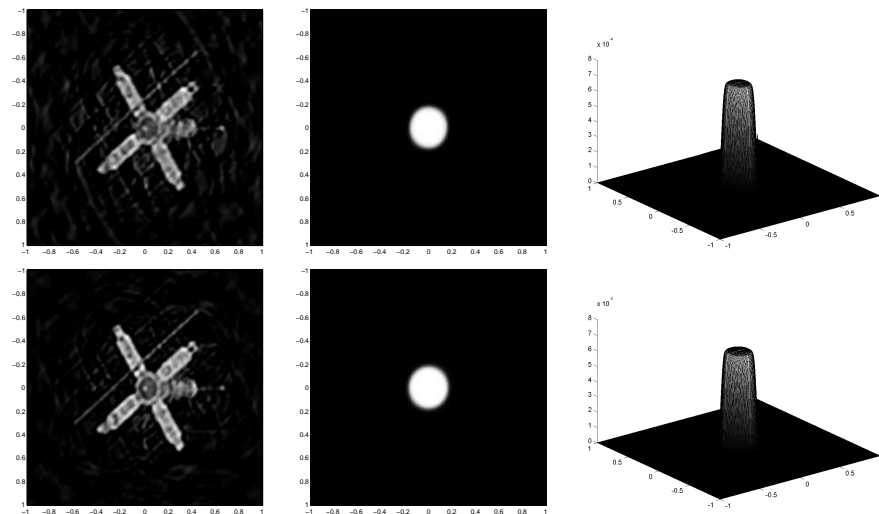


Figure 7: Recovered images (left), recovered PSFs (middle) and their corresponding 3D plots of the recovered PSFs (right) after one iteration (the upper one) and two iterations (the lower one).

recovered PSF is quite close to the original one. To further check these recovered results, we fix  $\alpha_2 = 6.4 \times 10^{-3}$  and vary  $\alpha_1$ . Fig. 6 shows the recovered images and the identified PSFs with their corresponding three-dimensional plots for varies  $\alpha_1$ . We see that the best recovered results are still obtained in Fig. 5. We also report that the number of iterations required for the alternating iterative algorithm is only two for this setting. In Fig. 7, we show the restored results and find that the recovered image and PSF are quite good after the first iteration.

As for a comparison, we test the following four settings:

(i) When the total variational regularization is used for both image and PSF, i.e.,

$$\min_{(u,k)} E(u,k) = \min_{u,k} \{ \|k * u - f\|_2^2 + \alpha_1 \int |\nabla u| + \alpha_2 \int |\nabla k| \},$$

the best recovered results are shown in Fig. 8. Although the quality of the recovered PSF is quite well, we obtain a recovered image with clear structure but little detail.

(ii) When the Lipschitz regularization is used for image and the  $H^1$ -norm regularization is used for PSF, i.e.,

$$\min_{(u,k)} E(u,k) = \min_{u,k} \{ \|k * u - f\|_2^2 + \alpha_1 (\|u\|_2 + \gamma \|z_t * u\|_2^2) + \alpha_2 \int |\nabla k|^2 \},$$

the best recovered results are shown in Fig. 9. The quality of the recovered image is acceptable, but the quality of the recovered PSF is poor. We also remark that the number of iterations required for the alternating iterative algorithm is 100 in order to obtain such results.

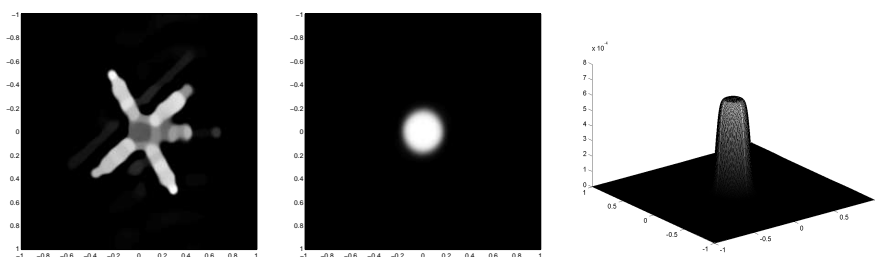


Figure 8: Recovered image (left), recovered PSF (middle) and the corresponding 3D plot of the recovered PSF (right) for  $\alpha_1 = 1.0 \times 10^{-5}$  and  $\alpha_2 = 5.10 \times 10^{-3}$  with the relative error of the recovered image = 0.3601 and ISNR=5.2903, and the relative error of the recovered PSF = 0.2841, where TV norm is used for both image and PSF.



Figure 9: Recovered image (left), recovered PSF (middle) and the corresponding 3D plot of the recovered PSF (right) for  $\alpha_1 = 2.01 \times 10^{-6}$  and  $\alpha_2 = 1.62 \times 10^{-4}$  with the relative error of the recovered image = 0.3618 and ISNR=5.2511, and the relative error of the recovered PSF = 0.2616, where Lipschitz regularization is used for image and  $H^1$ -norm regularization is used for PSF.

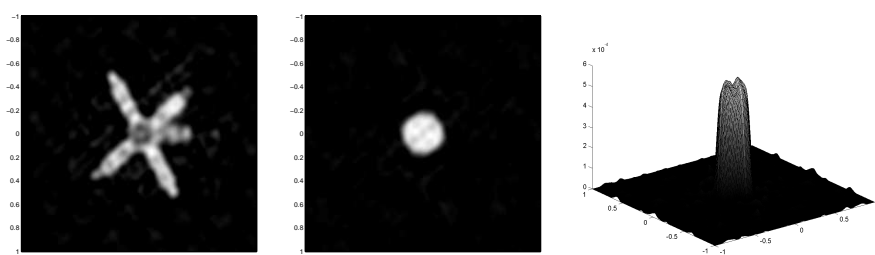


Figure 10: Recovered image (left), recovered PSF (middle) and the corresponding 3D plot of the recovered PSF for iterations=100,  $\alpha_1 = 1.20 \times 10^{-3}$  and  $\alpha_2 = 2.00 \times 10^{-3}$  with the relative error of the recovered image = 0.4376 and ISNR = 3.5987, the relative error of the recovered PSF = 0.3446, where  $H^1$ -norm regularization is used for both image and PSF.

(iii) When the  $H^1$ -norm regularization is used for both image and PSE, i.e.,

$$\min_{(u,k)} E(u,k) = \min_{u,k} \{ \|k * u - f\|_2^2 + \alpha_1 \int |\nabla u|^2 + \alpha_2 \int |\nabla k|^2 \},$$

the best recovered results are shown in Fig. 10. It is clear from this figures that both the quality of the recovered image and PSF are poor.

(iv) When the  $H^1$ -norm regularization is used for image and the total variational regular-

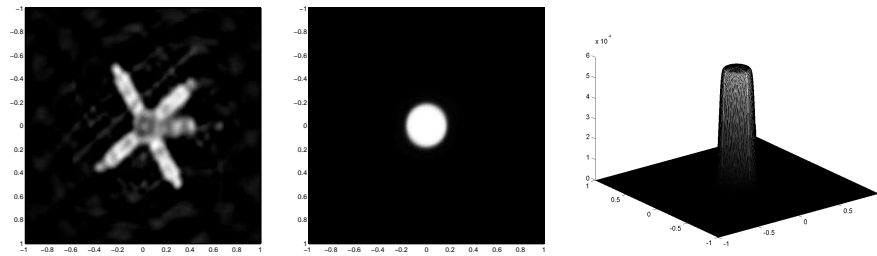


Figure 11: Recovered image (left), recovered PSF (middle) and the corresponding 3D plot of the recovered PSF for  $\alpha_1 = 10^{-3}$  and  $\alpha_2 = 8 \times 10^{-3}$  with the relative error of the recovered image = 0.3808 and ISNR=4.8059, and the relative error of the recovered PSF = 0.2469, where  $H^1$ -norm regularization is used for image and TV norm is used for PSF.

ization is used for PSF, i.e.,

$$\min_{(u,k)} E(u,k) = \min_{u,k} \{ \|k * u - f\|_2^2 + \alpha_1 \int |\nabla u|^2 + \alpha_2 \int |\nabla k| \},$$

the best recovered results are shown in Fig. 11. In this setting, though some texture appears, and the quality of the recovered PSF is quite good, it is much poorer than that in Fig. 5. We summarize that the relative errors of the recovered image and PSF (and the ISNR of the recovered image) by our proposed method are less (higher) than those of the above four settings.

## 4 Concluding remarks

Based on the assumption that images belong to proper Lipschitz spaces, the Lipschitz regularization method can recover images efficiently. In this paper, we introduce Lipschitz regularization method to image in blind deconvolution procedure, while the total variational regularization method is used for PSF. Because the excellent recovering effect of fine scales of image with Lipschitz regularization, the blind recovering image has more clear fine detail. The effects can be seen from the experiments we have done in Section 3.

## Acknowledgments

This research is supported in part by RGC 7046/03P, 7035/04P, 7035/05P and HKBU FRGs.

## References

- [1] A. A. Carasso, Singular integrals, image smoothness, and the recovery of texture in image deblurring, SIAM J. Appl. Math., 64 (2004), 1749-1774.

- [2] R. H. Chan, T. F. Chan and C. K. Wong, Cosine transform based preconditioners for total variation minimization problems in image processing, in: S. Margenov and P. Vassilevski (Eds.), *Iterative Methods in Linear Algebra, II*, IMACS Series in Computational and Applied Mathematics, V3, IMACS, NJ, 1996, pp. 311-329.
- [3] T. F. Chan and C. K. Wong, Total variation blind deconvolution, *IEEE Trans. Image Process.*, 7 (1998), 370-375.
- [4] R. A. Devore, B. Jawerth and B. J. Lucier, Image compression through wavelet transform coding, *IEEE Trans. Inf. Theory*, 38 (1992), 719-746.
- [5] R. A. Devore and B. J. Lucier, Classifying the smoothness of images: Theory and application to wavelet images processing, in: *Proceedings of the 1994 IEEE International Conference on Image Processing*, Austin TX, Vol. 2, IEEE Press, Los Alamitos, CA, 1994, pp. 6-10.
- [6] D. Fish, A. Brinicombe and E. Pike, Blind deconvolution by means of the Richardson-Lucy algorithm, *J. Opt. Soc. Am. A*, 12 (1995), 58-65.
- [7] Y. Gousseau And J.-M. Morel, Are natural images of bounded variation?, *SIAM J. Math. Anal.*, 33 (2001), 634-648.
- [8] L. He, A. Marquina and S. J. Osher, Blind deconvolution using TV regularization and Bregman iteration, *Int. J. Imag. Syst. Technol.*, 15 (2005), 74-83.
- [9] D. Kundur and D. Hatzinakos, Blind image deconvolution, *IEEE Sig. Process. Mag.*, 13 (1996), 43-64.
- [10] M. Ng, *Iterative Methods for Toeplitz Systems*, Oxford University Press, 2004.
- [11] C. Vogel and M. Oman, Iterative methods for total variation denoising, *SIAM J. Sci. Comput.*, 17 (1996), 227-238.
- [12] Y. You and M. Kaveh, A regularization approach to joint blur identification and image restoration, *IEEE Trans. Image Process.*, 5 (1996), 416-428.
- [13] Y. You and M. Kaveh, Anisotropic blind image restoration, *IEEE Int. Conf. Image Process.*, Lausanne, 1 (1996), 461-464.